A Predictive Control Scheme for Real-Time Demand Response Applications

Ioannis Lampropoulos, *Student Member, IEEE*, Nadina Baghină, Wil L. Kling, *Member, IEEE*, and Paulo F. Ribeiro, *Fellow, IEEE*

***Abstract*—In this work, the focus is placed on the proof of concept of a novel control scheme for demand response. The control architecture considers a uniform representation of non-homogeneous distributed energy resources and allows the participation of virtually all system users in electricity markets. The proposed scheme captures the operational planning, the real-time operations, the verification of the energy and service provision, and the financial settlement. The research involves the experimental verification of the proposed control and communication architecture between the aggregator and a system user in a laboratory environment. Emphasis is given on the real-time operations, whereas the case study is about the domestic freezer appliance. The convergence of the demand response system under load frequency control is investigated through simulation studies and the time response is compared to that of conventional balance suppliers in The Netherlands.**

***Index Terms*—Demand forecasting, power system control, predictive control, real time systems, supply and demand.**

I. Introduction

THE DEVELOPMENT of demand response (DR) mechanisms can provide a suitable option for the proper integration of renewable energy sources (RES) and the establishment of efficient generation and delivery of electrical power. DR can provide the means to limit the market power of conventional suppliers under conditions of resource scarcity, and to improve operational reliability in the presence of intermittent generation [1], [2]. DR encloses the planning, operation, monitoring and financial settlement of programs designed to incentivise end-users to alter their electricity usage patterns by scheduling in time and levelling the instantaneous power demand. The full potential of DR can be significant, but its exploration still remains a challenge, mainly due to the non-homogeneity and the distributed nature of energy resources.

Various control schemes for DR architectures have been proposed in the technical literature. Frequency-based control schemes can be used for primary frequency regulation and in autonomously operated systems [3]–[5]. However, in large synchronous systems, consisting of interconnected control areas, the provision of operating reserves for secondary control is governed by the *area control error* calculations [6], where the prevailing factor is the net difference between the actual and scheduled power interchange rather than the effect of frequency deviations. The idea of aggregating distributed energy resources for the provision of secondary operating reserves has been studied for the case of thermostatically controlled appliances through direct control schemes and centralised architectures in [7] and [8].

The power system was traditionally operated based on a centralised optimisation approach applied by the electric utility (e.g., through *automatic generation control*), and this organisation supported the development of direct control schemes. However, current developments with respect to market deregulation and the increasing integration of RES have stirred research activities from centralised to distributed and decentralised control schemes. In this context, the topic of price-based control is getting increasing attention [9]. Prices can be broadcasted in real-time to a number of system users under a specific control area (locational pricing) or connected to a network node (nodal pricing). In most of the references in the technical literature, which are dealing with real-time pricing, the focus is on utilising DR as an hourly energy resource [9], [10]. Even though the scheduling of the demand for electricity on an hourly basis can provide an efficient resource for many applications, the challenge is to shape the demand close to real-time to support primary and secondary frequency regulation, and network congestion management applications. Recent advances in information and communication technologies create new opportunities for the large-scale implementation of DR mechanisms and for close to real-time adaptation of the demand to optimise the power supply [11].

The main contribution of the paper is the proof of concept of the DR architecture proposed in [12], by utilising the model of the domestic freezer which is presented in [13] as basis for a case study. The proposed scheme considers a decentralised control structure and a uniform representation of non-homogeneous energy resources, since each resource is not distinguished from another based on its physical specifications and operational functions, but based on the characteristics of energy utilisation [12]. In this work, real-time applications for residential DR are defined which include participation and verification in wholesale electricity trade and real-time markets for ancillary services (i.e., provision of operating reserves for load frequency control). The objective function of an individual process and the control signal for real-time automated DR are formulated. The proposed control scheme is verified through experimental research and theoretical studies. The convergence of the aggregate DR system under load frequency control is investigated through computer simulations, and the results are compared with actual market and performance data from conventional balance suppliers in The Netherlands.

Manuscript received September 30, 2012; revised February 06, 2013 and March 28, 2013; accepted April 01, 2013. Date of publication May 29, 2013; date of current version November 25, 2013. This work was supported in part by the E-Price project (Price-based Control of Electrical Power Systems) funded by the European Commission's Seventh Framework Program.

The authors are with Electrical Engineering Department, Eindhoven University of Technology, The Netherlands (e-mail: i.lampropoulos@tue.nl; n.g.baghina@tue.nl; w.l.kling@tue.nl; p.f.ribeiro@tue.nl).

Digital Object Identifier 10.1109/TSG.2013.2257891

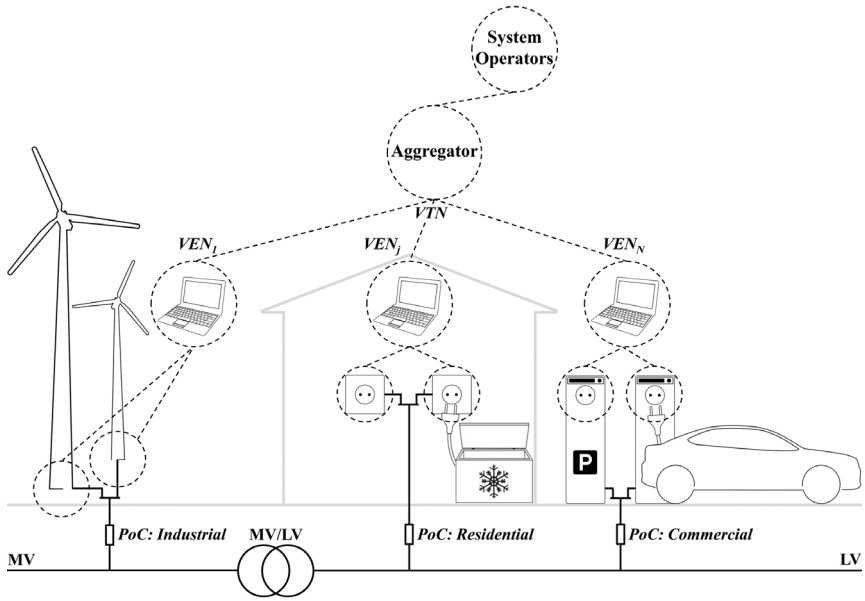

Fig. 1. Schematic of the operational architecture. The aggregator is the coordinator of a virtual power plant which consists of an aggregation of distributed energy resources. The black lines depict the physical power system and the points of connections (PoC) with system users, whereas the dashed lines represent the communication links between system entities.

The paper is structured as follows: Section II provides a description of the control system architecture and an overview of the system actors. In Section III the experimental setup and the implemented model-based predictive controller are described for the case study of the domestic freezer. Section IV is about aggregation of distributed energy resources through computer simulations, and in Section V the simulation results are presented and an assessment of the aggregate DR system is performed. The paper ends with discussion and conclusions.

II. System Design

An electrical power system consists of different control areas interconnected through high voltage (HV) synchronous or asynchronous connections. In Europe, each control area is operated by the transmission system operator (TSO), the legal entity that monitors the electricity network, ensures the connections with other control areas, and organises the markets for operating reserves and cross-border capacity. Regional distribution system operators (DSO) connect individual customers to the grid and provide the distribution of electricity. Medium voltage (MV) electrical networks are connected to low voltage (LV) networks through MV/LV transformer substations, which subsequently feed a large number of end-users at the LV level.

The main actors distinguished in this work are: the *system operators* (i.e., the operators of the electricity markets, and the transmission and distribution systems), the *aggregators* (legal entities that hold contracts with system users and coordinate them in real-time), and the *system users* (e.g., producers and consumers). In this article, an effort is made to keep terminology consistent with the definitions available in [14].

In the next sections, a decentralised control structure with a global coordinator is presented. The aggregator is the coordinator of a virtual power plant (VPP) which consists of an aggregation of distributed energy resources. In Fig. 1, the aggregator can be seen as a virtual top node (VTN), associated with a number of system users connected to the LV and MV grids. A system user can be seen as a virtual end node (VEN), which is defined as a device or system that can exchange communication signals and can also control electricity end-use and generation [15]. The focus is on the interactions between the aggregator and a number of associated system users (i.e., the VEN_j, with $j = 1, \ldots, N$).

III. Experimental Research

The experimental part of this research involves the empirical verification of the proposed communication and control architecture between the aggregator and an individual system user in a laboratory environment. The case study refers to a system user (e.g., VEN_j) who is associated with the jth process (i.e., the controllable domestic freezer). In this section, the implemented communication and control architecture are described, and the experience gained during the experimental verification is analysed.

A. The Experimental Setup

The experimental setup has been presented in [13], and comprised of three main parts: the sensing infrastructure, the communication infrastructure and the model-based predictive controller. The sensing infrastructure was put in place to monitor all the concerned parameters: the internal air temperature of the freezer and the ambient temperature were monitored through integrated temperature sensors, while the power demand was monitored by using an energy metering integrated circuit [16].

The communication infrastructure relied on the Zigbee low-power communication protocol which is based on the IEEE 802.15.4 standard [17]. An actuator, composed of a solid-state relay circuit, was controlling the freezer operation by turning its compressor *on* and *off* whenever it received a control signal from the implemented energy management system. The latter actually consisted of a computer which was the physical accommodation of the controller that was processing the measured

data and was defining the future inputs for the actuator based on a local optimisation problem. All software codes were written in Matlab [18].

During the laboratory experiments, all measurements were conducted on a per second basis, whereas the control actions were performed on a per minute basis. This is a distinct case compared to the computer simulations, described in Section IV-D, where both the time interval for performing the control actions and the sampling interval for analogue measurements is set to four seconds.

B. Model-Based Predictive Control

Model-based predictive control (MPC) refers to a class of control algorithms that utilise an internal model to predict the future response of a process [19], [20]. The freezer appliance operates in two states depending on whether the compressor is turned *on* or *off*. Given the state of the appliance, the developed software model of the freezer operation is based on a dynamic energy balance equation [21], which can be written as follows:

$$T(k+1)=\begin{cases} \varepsilon\cdot T(k)+(1-\varepsilon)\cdot(T_k^o-\frac{\eta\cdot p_k}{A}), & \text{when } \textit{on} \\ \varepsilon\cdot T(k)+(1-\varepsilon)\cdot T_k^o, & \text{when } \textit{off} \end{cases} \quad (1)$$

where $T(k+1)$ is the temperature inside the freezer at control period $k+1$, $\varepsilon=\exp(-\tau/\tau_c)$ is the factor of inertia, τ is the duration of the control period, $\tau_c=m_c/A$ is the time constant, m_c is the total thermal mass in $(\mathrm{W}h/^\circ\mathrm{C})$, A is the overall thermal conductivity in $(\mathrm{W}/^\circ\mathrm{C})$, T_k^0 is the ambient temperature in $(^\circ\mathrm{C})$ at control period k, η is the coefficient of performance, and p_k is the electrical power demand in (W) at control period k. Given the state of the appliance, the temperature inside the freezer is typically assumed to evolve according to a first-order ordinary differential equation [5], which can be written as follows:

$$\dot{T}(k)=\begin{cases} \dfrac{-A}{m_c}\cdot\left(T(k)-T_k^o+\dfrac{\eta\cdot p_k}{A}\right), & \text{when } \textit{on} \\ \dfrac{-A}{m_c}\cdot(T(k)-T_k^o), & \text{when } \textit{off}. \end{cases} \quad (2)$$

During computer simulations, described in Section IV, the electrical power demand p_k is assumed to be constant at 70 W when the state is *on*, and 0 W when the state is *off*. During the experimental phase, p_k is modelled as an exponential function to improve the forecast accuracy (See Fig. 2(b)), which can be written as follows:

$$p_k=\begin{cases} p_o\cdot\exp\left(-\lambda\cdot(k-k_o)\right)+p_c, & \text{when } \textit{on} \\ 0, & \text{when } \textit{off} \end{cases} \quad (3)$$

where p_o and p_c are power constants, $p_o=16\,\mathrm{W}, p_c=64\,\mathrm{W}$, k_o corresponds to the control period that signifies the beginning of the most recent *on* cycle, and $\lambda=1/340$ is the decay constant. The constants in (3) were defined based on experimental data. The developed model of the freezer operation was verified based on measurements obtained from the experimental setup [13].

The model-based predictive controller of the jth process receives in real-time an external signal from the aggregator which consists of a set-point trajectory $s(k+i|k)$ over a receding control horizon, $i=1,\ldots,i_{horizon}$. The notation $s(k+i|k)$ indicates that the set-point trajectory depends on the conditions at current time instant k [19]. The set-point trajectory $s(k+i|k)$ actually represents short-term requests for DR actions. Thus, when upwards regulation is requested the energy consumption of the freezer over the control horizon is minimised and the internal temperature of the freezer is kept on the upper temperature boundary, whereas when downwards regulation is requested the energy consumption is maximised and the internal temperature is kept close to the lower temperature boundary (See Fig. 2).

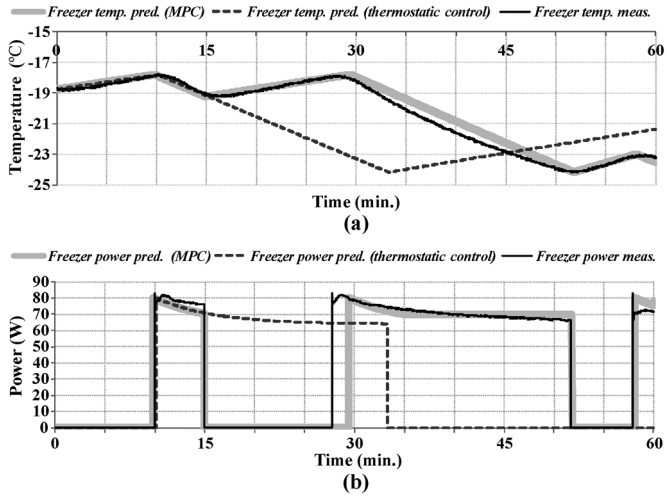

Fig. 2. Illustration of the real-time operation of the controllable freezer, considering that at current time $t=0\,\mathrm{min.}$ and until $t=30$ min. the aggregator requests upwards regulation (i.e., generation increase or load reduction), whereas from time $t=30$ min. and until $t=60$ min. the aggregator requests downwards regulation (i.e., load increase). (a) Predicted and measured temperature profiles. (b) Predicted and measured power profiles.

C. Optimisation Problem

MPC transforms a control problem into an optimisation problem, which can be solved over a prediction horizon, subject to system dynamics, an objective function, and constraints. Once the aggregator has broadcasted the set-point trajectory $s(k+i|k)$, then each system user can respond in a decentralised fashion based on a local optimisation problem. The jth system user performs a model-based optimisation over the control horizon and sends back to the aggregator the reference trajectory $r_j(k+i|k)$ about the part of the request that can be fulfilled. The reference trajectory of the jth process is equal to the difference between the optimised power output $p_{MPC,j}(k+i|k)$ under the MPC scheme, and the predicted power output $p_{th,j}(k+i|k)$ under the standard thermostatic control, over the control horizon, $i=1,\ldots,i_{horizon}$. The reference trajectory of the jth process can be written as follows:

$$r_j(k+i|k)=p_{MPC,j}(k+i|k)-p_{th,j}(k+i|k). \quad (4)$$

The objective of the optimisation that lies at the basis of the controller of the jth system user is formulated as a process that maximises the service provision offered to the aggregator (i.e., maximises the energetic contribution) over a time horizon of i steps, $i=1,\ldots,i_{horizon}$, starting at current discrete time control period k and subject to constraints, while contributing to the signal $s(k+i|k)$. In a classical MPC problem formulation, the objective function should account for the sum over the control horizon

$$\sum_{i=1}^{i_{horizon}} r_j(k+i|k).$$

However, in this work, a different approach is followed. The objective function of an individual user has been formulated to account separately for each discrete time interval i over the control horizon, and the optimised power profile $p_{MPC,j}(k+i|k)$ is generated in an iterative way. The optimisation goal is to minimise or maximise the objective function depending on the sign of the set-point trajectory and can be written as follows:

$$\begin{aligned} &\min_{u_j(k+i|k)} \{r_j(k+i|k)\}, \quad \text{if} \quad s(k+i|k) > 0 \\ &\max_{u_j(k+i|k)} \{r_j(k+i|k)\}, \quad \text{if} \quad s(k+i|k) < 0. \end{aligned} \tag{5}$$

Initially the controller of the jth process looks at the first time interval $i = 1$, over the control horizon, and depending on the sign of the set-point trajectory $s(k+1|k)$ defines the input $u_j(k+1)$ which satisfies the optimisation goal subject to constraints. The input $u_j(k+1)$ actually consists of a switching *on/off* command for the jth process (i.e., the jth freezer). Then the iteration step increases $i = i + 1$ and the whole process is repeated.

Therefore, the objective function reflects a voluntary nature, and even though the power profile $p_{MPC,j}(k+i|k)$ might not be optimal over the whole control horizon, the reason behind this design choice is twofold: first to provide a fast response to the aggregator's request, starting at the next control interval $k+1$, subject to constraints and the capabilities of the jth freezer at time instant k, and second to cope with the uncertainty related to the length of the control horizon since both the power system state and the domestic freezer operation are characterised by high dynamics. Furthermore, the freezer is characterised by low controllability due to the relatively low thermal inertia and the user intervention.

D. Operational Constraints

The operation of an individual freezer is locally controlled in order to comply with the request received from the aggregator, while dealing with system constraints and external influencing factors such as ambient temperature and user behaviour. The temperature limits inside the freezer are considered as hard constraints, to ensure that the stored food items are properly preserved. In quasi-steady-state operation, the evolution of the temperature T_j inside the compartment of the jth freezer is bounded within the range of $-24\,^{\circ}\mathrm{C}$ to $-18\,^{\circ}\mathrm{C}$.

Furthermore, in order to avoid any mechanical stress to the compressor that might be caused due to fast actuations, a minimum *on* operational time of five minutes is considered during the simulations and experiments. The constraints, related to the operation of the jth freezer, can be formulated as follows:

$$-24\,^{\circ}\mathrm{C} \leq T_j \leq -18\,^{\circ}\mathrm{C} \tag{6}$$

$$\tau_{on} \geq 5 \text{ min.} \tag{7}$$

E. Automated Demand Response

Automated DR refers to an automated notification process between the system operators and the system users. Considering an advanced sensing and communication infrastructure, automated functions can be effectively designed that require minimum user intervention [9].

The real-time operation of the experimental freezer, under automated DR, was demonstrated in a laboratory environment. Note that during the experimental phase of the research, the experiments were not designed to resemble the simulation scenario, which is described in Section IV, but those were designed to involve different conditions, time durations and control requests. In Fig. 7, a histogram of all the measured temperature samples (scaled up by a factor of 10^2) inside the compartment of the experimental freezer is presented. As can be seen in this histogram a number of the measured temperature samples from the experimental freezer fall outside the temperature limits formulated in (6). The temperature inside the experimental freezer was found to evolve within the range of $-24.65\,^{\circ}\mathrm{C}$ to $-17.54\,^{\circ}\mathrm{C}$, and the violations observed with the measurement data are attributed to the time interval of one minute for performing the control actions and the accuracy of the temperature sensors. During the laboratory experiments, the control actions were performed on a per minute basis which might allow the temperature inside the freezer to evolve over the temperature limits, whereas the temperature sensor placed inside the freezer compartment had an accuracy of $0.25\,^{\circ}\mathrm{C}$. Nevertheless, it is expected that in a designated practical system for real-time applications the control actions can be performed closer to real-time and operational constraints can be respected.

An example of the real-time operation of the experimental freezer is illustrated in Fig. 2, considering that the current time is $t = 0$ min. and the control horizon covers a period of one hour. In this example, from $t = 0$ min. and until $t = 30$ min. the aggregator requests upwards regulation (i.e., generation increase or load reduction), whereas from time $t = 30$ min. and until $t = 60$ min. the aggregator requests downwards regulation (i.e., load increase). As can be seen in Fig. 2, following the request from the aggregator at $t = 0$ min., the local model-based controller of the jth process (i.e., the controllable experimental freezer) optimises the short-term power demand of the appliance to minimise the energy demand until $t = 30$ min. and then to maximise the energy demand from $t = 30$ min. until $t = 60$ min., subject to constraints.

During the experimental phase of the research it was found that the objectives for DR can be in conflict with the general objectives for increasing efficiency, equivalently reducing electricity consumption. Specifically, when downward regulation is requested (equivalent to energy consumption maximisation), the freezer is commanded to operate close to the lower temperature boundary. Therefore, the average temperature difference between the interior of the freezer and the ambient environment is larger during downward regulation. This can be translated to higher energy losses due to convective heat transfer. Simulation results indicate that the daily energy consumption of the freezer is increased by approximately 10 % when downward regulation is performed throughout the day, given the ambient temperature T_k^o variations within the range of $20\,^{\circ}\mathrm{C}$ to $28\,^{\circ}\mathrm{C}$ in the laboratory environment. Contrary, when upwards regulation is performed, the daily energy consumption of the freezer is decreased by approximately the same percentage.

IV. Computer Simulations

The convergence of the aggregate DR system is investigated through computer simulations. In an effort to demonstrate the potential of utilising DR resources in real-time electricity markets, the developed scenario addresses the load frequency con-

TABLE I
NOMENCLATURE

i	Discrete step for control periods, i=1,..., n.
j	Index for system users and processes, j=1, ..., N.
k	Current discrete time control period.
l	Discrete step for the settlement periods, l=1,..., m.
$p_j(k+i\|k)$	Power trajectory of the jth process (W).
$p(l)$	Schedule for the day ahead (W).
$r_j(k+i\|k)$	Reference trajectory of the jth process (W).
$r(k+i\|k)$	Aggregate reference trajectory (W).
$s(k+i\|k)$	Processed set-point trajectory (W).
$T_j(k+i\|k)$	Internal temperature trajectory of the jth process (°C).
$u_j(k+i\|k)$	Input trajectory of the jth process.
$w_j(k)$	Binary notification signal.
$y_j(k)$	Power output of the jth process (W).
$y(k)$	Aggregate power output (W).
$z(l)$	Power imbalance (W).
τ, τ_c, τ_s	Time intervals (s).

trol (LFC) coordinated by the TSO. For the convenience of the reader a simulation pseudo code for the real-time operations is provided in the Appendix that should be interpreted in parallel with the descriptions in Sections III–C and IV–D. Furthermore, in Table I, a nomenclature list is provided which includes the main notation of the paper for quick reference, whereas other symbols are defined as required throughout the text.

A. Simulation Scenario

For analysing the response of the aggregate DR system, the developed simulation scenario focuses on The Netherlands and covers a period of 24 hours. During the operational planning (*a priori*), which is described in Section IV-C, the timescale corresponds to discrete time periods of 15 minutes, in line with the defined settlement periods for energy scheduling and verification in The Netherlands. During real-time operation, which is described in Section IV-D, the time interval for simulations and for sampling analogue measurements is set to 4 seconds, inspired by the Dutch system design for LFC.

The underlying business model in the developed scenario sets distinct roles among all system actors. The aggregator represents, up to markets and the system operators, one thousand residential customers equipped with controllable freezers. Emphasis is given on the operational planning with respect to the day-ahead auction in The Netherlands [22], and the real-time market for operating (frequency restoration) reserves which is organised by the Dutch TSO [6]. The interactions between the system actors during the operational planning, the real-time operations under LFC, and the verification process are further discussed in the following paragraphs.

B. The Load Profile

In order to assess the performance of the aggregate DR system, it is important to create a realistic representation of the aggregate residential load in terms of energy volumes and time schedules. The aggregate power demand can be distinguished between the non-controllable base load and the controllable load due to the domestic freezers. The base load profiles that are incorporated in the simulation model are constructed based on representative electricity use patterns from a sample of Dutch households, and are verified based on actual data from a Dutch DSO [23]. The aggregate load profile of the domestic freezers is constructed based on the model described in Section III-B. For performing the day-ahead simulation, a population of 1000 freezers is commanded to operate under standard thermostatic control for two consecutive days. The reason for running the algorithms for two days sequentially is to initialise the simulation model during the first day and to randomise the states of the freezers to obtain a realistic aggregate behaviour during the second day. The results of the first day of simulation are discarded whereas the states and internal temperatures of the population of freezers at the beginning of the second day of simulation are recorded in two vectors for further use in the real-time simulations. The power demand predictions of individual freezers for the second day of simulation are added up to generate a vector representing the aggregate power demand of the controllable freezers under standard thermostatic control. Based on this vector, the day-ahead energy schedule, which is further discussed in Section IV-C, is generated.

The user intervention has also been integrated in the model by analysing the impact of door openings and thermal mass variations, based on experimental data [13]. Other disturbances due to external conditions (e.g., ambient temperature variations) are measured and consist of an input of the disturbance model which subsequently feeds the controller and the process model. Thermal mass m_c values corresponding to minimum, medium and maximum load are equally distributed among the population of freezers. The user intervention is assumed to occur in three distinct forms through door openings (with minimum impact on the thermal mass), load introduction (with a higher impact on the thermal mass), and load removal (with an impact equivalent to a door opening and a slight effect on the duration of the *on* and *off* periods). The user intervention is simulated based on data reported in [24] about the daily frequency of door openings of refrigerator systems in European households. Given the fact that, compared to refrigerator systems, freezers are less exposed to user intervention [24], the data were adapted and a certain distribution of door openings during a period of 24 hours is assumed for the population of simulated freezers. Data regarding the introduction of new load into the freezers are also integrated in the model by assuming a certain amount of load introduction per freezer and per week. Every time that new load is introduced, this is assumed to be equivalent to one kilogram of water at room temperature. Fig. 3(a) depicts the simulated load profile for 1000 households, distinguishing between the base load and the aggregate load of the domestic freezers.

C. Day-Ahead Planning

During the operational planning the aggregator defines an energy schedule $p(l)$ for the day-ahead which is actually a piecewise constant function with a finite power value for each settlement period $l = 1, \ldots, 96$, whereas the duration of the settlement period is 15 minutes. The energy schedule $p(l)$ represents the energy volumes which have been cleared through long-term (forward and future markets) and short-term trade (spot markets), and an example is illustrated in Fig. 3(a). The energy schedule is constructed based on individual prediction signals that are sent from the system users (i.e., the VEN_j, with $j = 1, \ldots, N$) to the aggregator, and cover a period of 24 hours

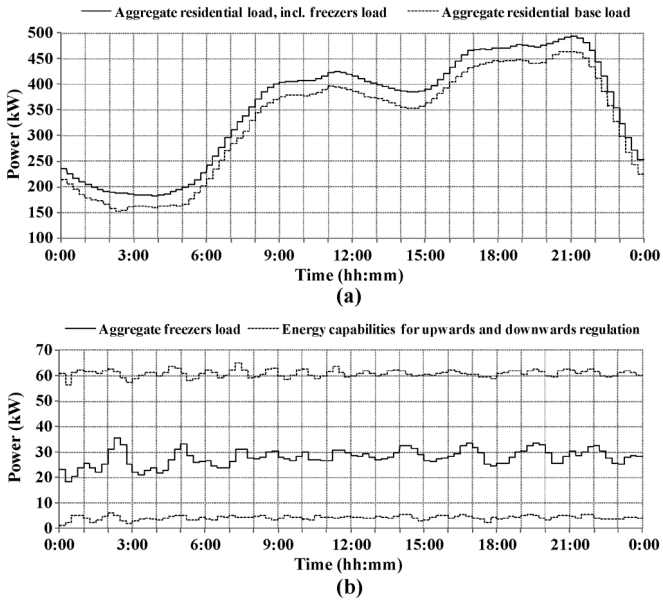

Fig. 3. Simulated aggregate load profiles in 15 min. time intervals for one thousand households equipped with controllable freezers. (a) The residential base load and the aggregate load including the freezers load. (b) Aggregate freezers load and energy capabilities for the provision of operating reserves.

starting at the time instant that indicates the beginning of the first control period of the operational day.

Following the clearing of the day-ahead market [22], the system users submit to the aggregator their energy capabilities for ancillary services, i.e., for the provision of operating (frequency restoration) reserves [6]. For the case of the domestic freezer that is represented by the jth system user (i.e., the VEN_j), the energy capabilities for upwards and downwards regulation correspond to the minimum and maximum energy consumption that can be achieved by the jth process. These energy capabilities are calculated for each lth settlement period separately, considering that the investigated DR system is in steady-state at the $(l-1)$th settlement period.

The aggregator collects and processes all information from associated system users, creates aggregate bids for frequency restoration reserves, and submits these bids to the operator of the real-time balancing market. The bids for frequency regulation reserves are in the form of a piecewise constant function with a finite value for each settlement period of the day-ahead. Note that the settlement periods for the day-ahead market and the real-time balancing market are distinct. However, in this work the same duration is assumed (i.e., 15 min.) and is denoted by the same symbol τ_s.

An example of the aggregate energy capabilities of the investigated DR system for the provision of operating reserves is given in Fig. 3(b), both for upwards and downwards regulation. Note that the plotted curves of energy capabilities for frequency regulation in Fig. 3(b) should not be directly interpreted as formulated bids to be submitted to the market for operating reserves. Actually, the aggregator should implement a strategy about transforming the energy capabilities for upwards and downwards regulations into market bids for operating reserves. This strategy should aim in the efficient utilisation of the aggregate DR resource. Since the demand for electricity varies as a function of time, the capacity that can be provided from DR mechanisms is also subjected to the timing and the duration of the request. In the case that a bid corresponding to the lth settlement period is activated, then the bids in consequent settlement periods will be affected. The latter holds especially for DR actions provided by controllable loads since a regulation-up or regulation-down action at time instant k will influence the functional specifications and energy capabilities at subsequent time intervals $k+i$, where $i=1,\ldots,n$. Therefore, the available DR capacity is relatively erratic and it is essential to continuously maintain a forecast of resource availability. In the case that the DR capacity is almost depleted, e.g., due to long and large request for regulation, then it is important for the aggregator to submit updated bids for frequency restoration reserves to the system operator.

D. Real-Time Operations

The proposed scheme is based on feedback control at the aggregator (i.e., the VTN) and distributed model-based predictive control at each associated system user (i.e., the VEN_j). The real-time operation, under the proposed control scheme, is illustrated in Fig. 4 where it is assumed that each VEN_j represents only one process. For example, the jth VEN (e.g., a residential customer) has an internal model which is used to predict and optimise, in a decentralised fashion, the jth process output $y_j(k)$ (i.e., the jth freezer power demand) over a prediction horizon of discrete steps $i=1,\ldots,n$, starting at current discrete time control period k. In a discrete time control procedure, the calculations take place at discrete steps which are defined by the time interval τ for simulations and for sampling analogue measurements. In this work, a 24 hours period with a time interval of $\tau=4$ s corresponds to $n=21\,600$ discrete time control periods.

In the proposed control scheme [12], the aggregator defines in real-time a processed set-point trajectory $s(k+i|k)$, and broadcasts this signal to all associated VEN (under a certain control area) at current discrete time control period k. Then, each system user can decide internally and in a decentralised manner how to respond to this control signal. The trajectory $s(k+i|k)$ actually represents the short-term objectives for DR, and is constructed based on information about: real-time requests from system operators for the provision of ancillary services, short-term predictions regarding the system state, and past control errors. Past control errors refer to deviations from the submitted energy schedule $p(l)$, where $l=1,\ldots,96$, for each settlement period of the operational day, whereas the real-time requests from system operators can refer, among others, to the TSO signals for LFC. To represent the TSO requests towards the aggregator, and to simulate the LFC signal, actual data of TenneT, the Dutch TSO, are utilised [25]. The actual LFC signal is scaled down, within the range of ± 20 kW (See Fig. 6(b)), to fit the nominal capacity of the aggregate DR system (See Fig. 3(b)).

The processed set-point trajectory $s(k+i|k)$ consists of the sum of two trajectories: a short-term prediction trajectory of the power deviation values $\delta p(k+i|k)$ which accounts for LFC requests, and a power deviation trajectory $dp(k+i|k)$ which accounts for corrective actions in the case of deviations from the

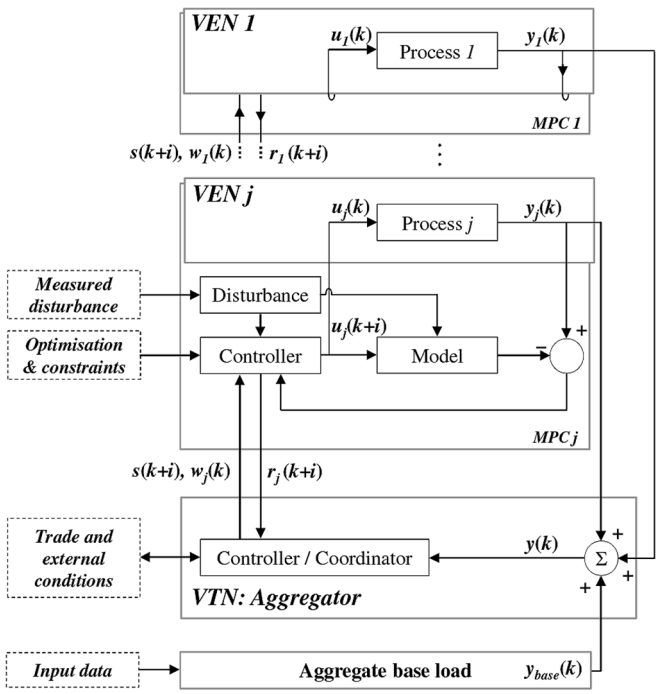

Fig. 4. The simulation model illustrating the real-time operations at discrete time control period k. The VTN represents the aggregator, whereas the jth VEN is illustrated together with the MPC block.

defined energy schedule $p(l)$. The processed set-point trajectory can be written as follows:

$$s(k+i|k) = \delta p(k+i|k) + dp(k+i|k). \tag{8}$$

Since the focus of this work is not on the forecasting methods, it is assumed that a perfect forecast of the $\delta p(k+i|k)$ trajectory is available, resembled by the actual data of the Dutch TSO. In a real life application, a short-term forecast of the LFC signal can be generated based on time series prediction methods. For the base load demand, it is assumed that the real-time power demand is equal to the forecast of the day-ahead, illustrated in Fig. 3(a). The aggregate base load $y_{base}(k)$ is summed up, at the aggregator level (See Fig. 4), with the power demand of all the controllable freezers $y_j(k), j = 1, \ldots, N$. During computer simulations, it is assumed that the internal software model of the jth process also creates a perfect forecast for the power demand $y_j(k)$ of the jth freezer.

The power deviation trajectory $dp(k+i|k)$ is defined by the aggregator in real-time based on an energy balance equation for each lth settlement period $l = 1, \ldots, 96$, that incorporates the defined energy schedule $p(l)$, the actual VPP output $y(i)$ up to current discrete time control period k, and the energetic contribution due to the LFC signal $\delta p(i)$. Starting at the beginning of the lth settlement period and up to the current discrete time control period k, the difference between the submitted energy schedule $p(l) \cdot \tau_s$ and the delivered energy (sum of the aggregate output but excluding the energy content due to the LFC requests) defines the energy content that must be delivered until the end of the lth settlement period (i.e., the product $v(k) \cdot (l \cdot \tau_s - k \cdot \tau)$). This can be expressed through an energy balance equation as follows:

$$p(l) \cdot \tau_s - \sum_{i=i_l}^{k} (y(i) - \delta p(i)) \cdot \tau = v(k) \cdot (l \cdot \tau_s - k \cdot \tau) \tag{9}$$

where $i_l = 225 \cdot (l-1) + 1$corresponds to the first control period of the lth settlement period, whereas the aggregator has to comply with the submitted energy schedule $p(l), l = 1, \ldots, 96$, for each settlement period ($\tau_s = 15$ min.) of the operational day. The value $v(k)$, calculated at current discrete time control period k, actually defines a new power set-point for the remaining time until the end of the lth settlement period that accounts for any energy imbalance up to time instant k. The power deviation trajectory can be formulated as follows:

$$dp(k+i|k) = v(k) - p(l) \tag{10}$$

where $i = 1, \ldots, 225 \cdot l - k$, whereas the values $v(k)$ and $p(l)$ in (10) have to be reset for all the control periods over the prediction horizon that correspond to the $(l+1)$th settlement period, i.e., for $i = 225 \cdot l - k + 1, \ldots, i_{horizon}$.

The aggregator defines and broadcasts in real-time the processed set-point trajectory $s(k+i|k)$ to all associated system users (i.e., the VEN_j, with $j = 1, \ldots, N$). Each individual VEN_j obtains the trajectory $s(k+i|k)$, and checks based on predictions whether it can partially contribute to the requested action. Then, the VEN_j sends back to the aggregator the individual reference signal $r_j(k+i|k)$ which includes the information about the part that can be fulfilled. The aggregator receives the signal $r_j(k+i|k)$ and performs consistency checks (e.g., overshooting avoidance). Then, sends back to the VEN_j a discrete binary signal, i.e., $w_j(k) \in \{0, 1\}$, to indicate rejection or acceptance with respect to $r_j(k+i|k)$. In case of acceptance, the VEN_j performs the control action and the first input is applied in the jth process. Subsequently, the aggregator subtracts the performed and planned actions (based on the sum $r(k+i|k) = \Sigma_j r_j(k+i|k)$) to maintain a forecast of changing conditions over the prediction horizon, re-calculates and forwards the updated processed set-point trajectory $s(k+1+i|k+1)$ and the whole process is repeated. This is called the receding horizon strategy, since the prediction horizon remains of the same length [19]. The aggregate net power use and generation at current discrete time control period k is the VPP output $y(k) = \Sigma_j y_j(k) + y_{base}(k)$. The aggregator's goal is to control the future power output $y(k+i)$ according to market contracts (cleared volumes on long-term and short-term markets) and the real-time requests from system operators [12].

E. Time Response Delay

Advances in communication network technology can enhance the development of real-time control and automation schemes. However, closed-loop control systems, especially via the Internet, are very difficult to implement practically due to their stochastic nature [11].

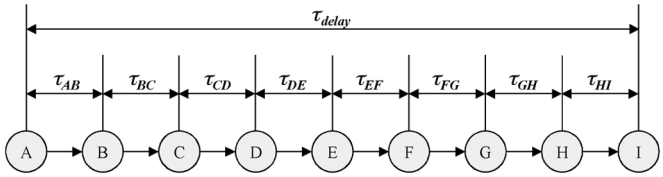

Fig. 5. Time sequence of a control cycle. A: Instant at which the system operator sends the value $\delta p(k)$ to the aggregator. B: Instant at which the aggregator receives the packet. C: Instant at which the aggregator sends the signal $s(k+i|k)$ to the system users. D: Instant at which the jth system user receives the packet. E: Instant at which the jth system user sends the signal $r_j(k+i|k)$ to the aggregator. F: Instant at which the aggregator receives the packet. G: Instant at which the aggregator finalises the consistency check and sends the signal $w_j(k)$ to the jth system user. H. Instant at which the jth system user receives the packet. I: Instant at which the actuator of the jth process receives and applies the future control input sequence.

The computational time delays due to algorithmic optimisation and the time delays caused by data transmission can impact the performance of the control system. Taking as a reference the time instant that the TSO sends the LFC signal to the aggregator, the actual provision of the requested operating reserves will occur with some inevitable time delay (i.e., the *time response delay*) mainly due to physical limitations. Therefore, in a practical system, it is important to account for computational and communication time delays.

The time sequence of a full control cycle between the aggregator and an individual system user is shown in Fig. 5. A control cycle is initiated by the system operator sending a request to the aggregator (i.e., the value $\delta p(k)$). At the same time, the aggregator calculates the aggregate power output $y(k)$ and subsequently defines and broadcasts the set-point trajectory $s(k+i|k)$ to all individual system users. Then, the jth system user performs a model-based optimisation of the jth process over the control horizon, $i = 1, \ldots, i_{horizon}$, and sends back to the aggregator the reference signal $r_j(k+i|k)$ about the part of the request that can be fulfilled. The aggregator receives the individual reference signal from the jth system user, checks if the aggregate response is larger than the actual request, and subsequently accepts (or rejects) the reference signal by sending back to the jth system user the binary notification signal $w_j(k)$. In case of acceptance, the jth system user performs the control action by applying the first input to the jth process. The total time delay of a control cycle can be written as follows:

$$\tau_{delay} = \tau_{AB} + \tau_{BC} + \tau_{CD} + \tau_{\mathrm{DE}} + \tau_{EF} + \tau_{FG} + \tau_{GH} + \tau_{HI} \tag{11}$$

where τ_{delay} is the total time delay for a full control cycle, τ_{AB}, τ_{CD}, τ_{EF}, τ_{GH}, τ_{HI} refer to the one-way delay between two synchronised points of an IP network, τ_{BC} is the computational time at the aggregator side for defining the set-point trajectory $s(k+i|k)$, τ_{DE} is the computational time at the system user side, (including time delay in the channel between the sensor and the controller), and τ_{FG} is the computational time at the aggregator side for performing consistency checks.

At the aggregator side, the computational time τ_{BC} for defining the set-point trajectory and the computational time τ_{FG} for checking the reference signal of the jth system user are considered as negligible. The computational time τ_{DE} due to optimisation of the jth process, i.e., for generating the predictions of one hour for the power and temperature profiles of the jth freezer, was calculated by using matlab measures for performance and was found to be 0.47 seconds.

In telecommunication systems the network latency in a packet-switched network is often measured round-trip. In [11], experimental results show that for internet-based control, where the controller and plant sides are placed at different locations, the round-trip time delay between the two sides varies from 0.32 to 0.56 s, for the case where the plant side is located in Europe while the controller side is located in Asia. Therefore, assuming a one-way time delay of 0.50 s can be considered as a conservative assumption.

In order to account for the above mentioned time delays, in this work it is assumed that the total time delay due to data transmission and computational time accounts for 8 s in total. Given the reported figures in literature, and calculated values from the implemented experimental controller, it can be stated that the assumed time delay of 8 s is considered realistic but rather conservative at the same time.

F. Verification and Financial Settlement

The verification of the service provision by the TSO and the financial settlement by the market operators are performed *a posteriori*, i.e., after the operational day. Any imbalance with respect to the submitted energy schedule $p(l)$ must be internally solved by the aggregator before the end of the lth settlement period, or settled with the TSO through the imbalance settlement [6]. This can be expressed through the following equation:

$$\sum_{i=i_l}^{225\cdot l} (y(i) - \delta p(i)) \cdot \tau - p(l) \cdot \tau_s = z(l) \cdot \tau_s \tag{12}$$

where $i_l = 225 \cdot (l-1) + 1$ corresponds to the first control period of the lth settlement period, whereas the aggregator has to comply with the submitted energy schedule $p(l), l = 1, \ldots, 96$, for each settlement period of the operational day, while excluding the energetic contribution due to LFC requests. However, any mismatch from the submitted schedule will be regarded as an imbalance $z(l)$ for the lth settlement period.

For the verification of the provision of operating reserves by the TSO, apart from the real-time measurements of the VPP output $y(k)$, a reference value is required, which must be sent by the aggregator to the TSO just before realisation. This reference value indicates the planned output of the VPP at a specific time instant in the short-term future, so that the TSO can check whether the aggregator actually delivered the real-time requests (e.g., for the provision of fast operating reserves). This reference value can be calculated within the VTN block (i.e., the aggregator) based on the day-ahead prediction signals, the incoming signals $r_j(k+i_{ref}|k)$ from each individual VEN_j and by using the following equation:

$$r(k+i_{ref}|k) = \sum_{j=1}^{N} r_j(k+i_{ref}|k) \tag{13}$$

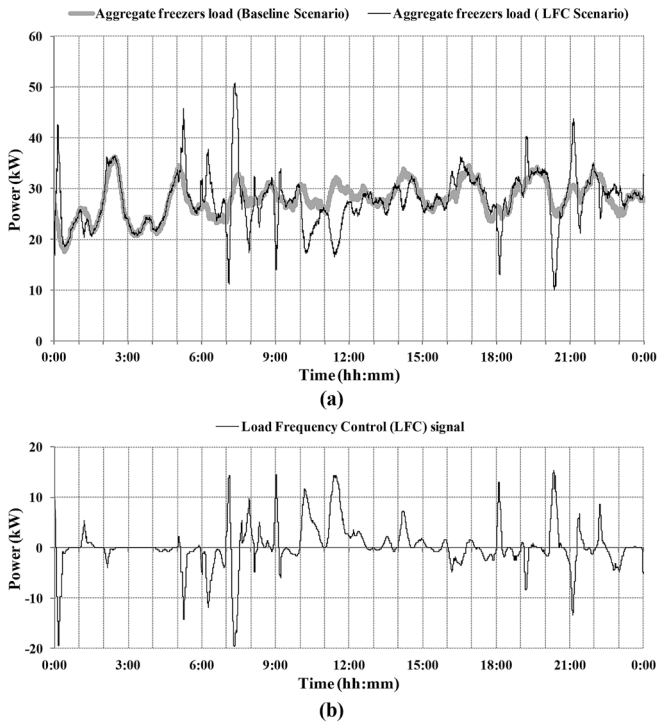

Fig. 6. Simulation results for the aggregate demand response system consisting of one thousand controllable freezers and for a period of twenty-four hours. (a) Power profiles for the aggregate freezers load for both the baseline and the LFC scenarios. (b) The load frequency control (LFC) signal.

where i_{ref} is a constant that determines a number of subsequent control periods. Considering the time interval τ for simulations, then the product $\tau \cdot i_{ref} = \tau_{ref}$ defines the time period between forwarding this reference value to the TSO and the actual realisation. The aggregator has an interest to keep this time period as short as possible, to have the opportunity to act on fast changing conditions. In The Netherlands, this time interval τ_{ref} has been set to one minute for conventional balance suppliers [6].

The financial settlement between the aggregator and associated system users is based on bilateral contractual agreements. The aggregator can organise and operate an internal single-sided market for system users, and the specific agreements can vary depending on the system users' preferences. For example, system users can participate in the aggregator's single-sided market under a pay-as-bid scheme or on a voluntary basis. Especially for residential customers that have limited capacity and controllability over the processes that run within their premises, the aggregator can define tailored DR programs that incentivise participation and at the same time provide a protective pricing environment [12].

V. Simulation Results

A. Demand Response Under Load Frequency Control

Simulation results of the real-time operation are given in Fig. 6(a), where the power profiles of the aggregate DR system, consisting of the controllable freezers, for both the *baseline scenario* and the *simulation scenario* are plotted. In this figure, the simulated power profiles should be interpreted in parallel with the LFC signal plotted in Fig. 6(b). Overall, there is a high anticorrelation between the resulted load profile in the *simulation scenario* and the LFC signal, with respect to the scheduled load of the freezers in the *baseline scenario*. As can be seen in Fig. 6, the aggregate demand is increased when down-regulation is requested and vice versa. Convergence is overall achieved, but when the LFC signal changes significantly within short time periods then some deviations are observed, with respect to the requested DR actions, and these deviations are related to the artificially incorporated time delay of 8 s, as described in Section IV-E. Still, the correlation between the control requests and the response of the aggregate DR system is relatively high for the simulation period of 24 hours and detailed results are presented in Section V-C.

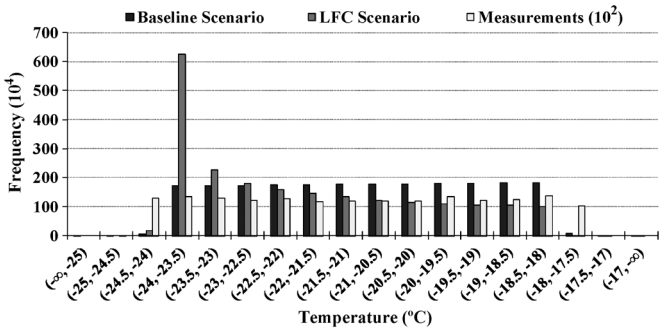

Fig. 7. Histogram of temperature samples from the performed simulations and the conducted measurements with the experimental freezer under automated demand response mode.

Simulation results demonstrate the capability of the DR system to flexibly shape the load, since the controllable freezers can cope with the LFC requests, and provide operating reserves with almost no ramp limitations. However, when the controlled period is prolonged, the DR system composed of the controllable freezers cannot cope with a long and large request for upwards or downwards regulation. In the latter case, a large number of freezers get synchronised, the aggregate resource is depleted and the DR system becomes unstable. The aggregator must define the range of the control signal appropriately to fit within the capabilities of the aggregate DR system. In order to achieve this, the operator has among other tools, the forecast over the receding horizon to check whether the DR system might reach an unstable condition at the end of the receding horizon due to depletion of the DR resource, and can command preventive actions to avoid that situation.

B. Operational Constraints

In Fig. 7, a histogram of temperature samples is presented both for the simulation data and the measurements with the experimental freezer under automated DR mode.

As explained in Section III-E, during the laboratory experiments, a relatively large number of measured temperature samples was observed to deviate within 0.5 °C over the temperature limits and these violations are attributed to the accuracy of the temperature sensors and the duration of the time interval for performing the control actions.

Regarding the simulation results, as can be seen in Fig. 7, the temperature constraints in the cooling compartment of individual freezers are satisfied under the LFC scenario. A

relatively small number of samples was observed outside the temperature limits formulated in (6), and these marginal violations are related to the user intervention and time delays. As explained in Section IV-B, the user intervention is also integrated in the model based on available data from European households and certain assumptions about user behaviour. User intervention occurs through door openings, load introduction, and load removal. In the situation that the door of a freezer is opened then the temperature inside that freezer rises due to the heat input of exchanging air, which can drive the temperature T_j up to $-15\,^{\circ}\mathrm{C}$. This was verified during simulation tests with the user mode switched off.

Finally, some marginal violations, i.e., less than $0.05\,^{\circ}\mathrm{C}$, over the temperature limits occur due to the artificially incorporated time delay of 8 s, as described in Section IV-E. In the case that the temperature inside a freezer is close to the lower or upper temperature boundary then it can be expected that the temperature limits can be marginally surpassed due to this artificially incorporated time delay.

C. Time Response Delay

Determination of the response delay is one of the main aspects involved in the process of assessing the service provision. In [6], an analysis tool is presented for defining the *time response delay* of a balance supplier, following a request of the TSO for the provision of operating reserves, by applying signal analysis. Based on the same analysis tool, the response of the aggregate DR system is assessed and simulation results are compared with actual data for portfolio-based balance suppliers in The Netherlands. The input data for this analysis were provided by TenneT, the Dutch TSO, and consist of daily profiles of anonymous balance suppliers with a resolution of 4 s for a random day of 2011. The daily profiles were split into hourly profiles and were assessed separately. The approach to determine the *time response delay* is by calculating the correlation coefficients between two variables which correspond to the two input signals in the verification process: *i*) the sum of the LFC signal and the scheduled power output, and *ii*) the actual power output of the balance supplier and the DR system. By time-shifting respectively the two signals with discrete steps (time-lags) and calculating the correlation coefficients, the *time response delay* is expected to be reflected at the corresponding time-lag where the correlation coefficient is maximised [6]. Given the fact that the discrete time step in the considered control procedure is $\tau = 4$ s, then the defined *time response delay* will always be a multiple of this time interval.

A representative sample of the results is plotted in Fig. 8, and presented in Table II. The grey coloured cells in Table II identify the higher performance, either in terms of higher achieved correlation between the time series, or in terms of lower *time response delay*. Simulation results show that the response of the aggregate DR system outperforms that of the conventional balance supplier, both in terms of higher achieved correlation, but also in terms of faster time response. The time response of the conventional balance supplier was calculated to vary between 8 to 88 s, for the investigated day [6], whereas the time response of the DR system was found to be 8 s, in line with the considered

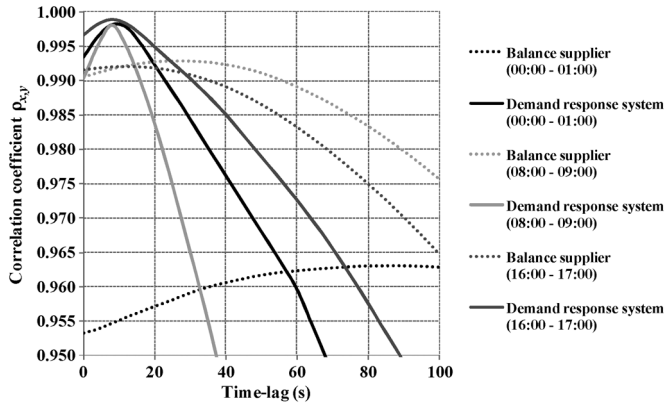

Fig. 8. Correlation coefficients for the two verification signals and for different time-lags. Plotted results include both cases of a conventional balance supplier and the simulated aggregate demand response system.

TABLE II
DEFINED CORRELATION COEFFICIENTS AND TIME RESPONSE DELAYS FOR A CONVENTIONAL BALANCE SUPPLIER AND THE DEMAND RESPONSE SYSTEM

	Balance supplier		Demand response system	
Time period	**Max. correl. coeff. (-)**	**Delay time (s)**	**Max. correl. coeff. (-)**	**Delay time (s)**
00:00 - 01:00	0.9630	88	0.9981	8
04:00 - 05:00	0.9589	8	0.9998	8
08:00 - 09:00	0.9929	28	0.9981	8
12:00 - 13:00	0.9481	16	0.9987	8
16:00 - 17:00	0.9921	12	0.9990	8
20:00 - 21:00	0.9930	16	0.9997	8
23:00 - 24:00	0.9967	8	0.9971	8

hypotheses for a total of 8 s of minimum time delay. Simulation results show that the DR system can shape the load profile in a flexible way, and provide secondary frequency regulation reserves almost with no ramp limitations.

VI. DISCUSSION

Experimental and simulation results indicate that the selected case study of the domestic freezer has relatively low capabilities for energy storage but can be ideal for short-term DR. However, when the controlled period is prolonged, the DR system composed of controllable freezers cannot cope with a long and large request for upwards or downwards regulation. The ideas described in this paper can be extended to address other thermostatically controlled appliances, characterised by larger capabilities for energy storage, such as industrial freezers and space-conditioning systems.

Relevant topics for future research would be to consider a diversified portfolio of electrical loads and distributed generators for the aggregator, and to investigate the effect of markets for the provision of localised ancillary services. In this context, the proposed control scheme can be extended to capture also reactive power control. The aggregator can define and broadcast, next to the set-point trajectory for active power, a set-point trajectory for reactive power control. Then, distributed resources such as inverters which connect distributed generation and chargers for electric vehicles [26], could provide reactive power support to the power system.

An economic assessment of a residential DR system has been performed for the case of the aggregator participating in the Dutch day-ahead auction and the real-time market for operating (frequency restoration) reserves, and the results have been presented in [23]. Residential DR can become an interesting business case for new entities in the energy market. Primary, the aggregator is expected to take advantage of price differences between forward, future, spot markets and the retailing price for electricity. The aggregator can utilise the controllable loads to reduce risks while planning under uncertainty, especially with respect to the integration of intermittent generation, whereas participation in ancillary services markets can provide additional revenues.

In this work, the objective function of an individual user has been defined to reflect a voluntary nature. Future research on the proposed control scheme could incorporate prices. In a price-based control scheme, the energy schedules, energy capabilities and real-time requests for operating reserves should be accompanied with prices. Then the objective function can be formulated as a cost function, whereas the optimisation goal shall be the minimisation of costs, or a profit function with the optimisation objective to maximise profits and revenues from trading electricity in wholesale markets and participating in markets for ancillary services.

Finally, privacy concerns can influence significantly the user acceptance with respect to the development of DR applications. In the proposed control scheme, the decentralised decision making which occurs at the local controllers ensures that no sensitive data, related to user behaviour, requirements and schedules, are transmitted outside the premises of a system user. All local objectives and constraints are processed locally and only aggregate and reference data are communicated with the aggregator and system operators.

VII. Conclusions

In this article, a novel control scheme for automated demand response mechanisms is demonstrated through experimental research and computer simulations. The proposed scheme considers a decentralised control structure, a uniform representation of non-homogeneous resources, automated functions, and distributed intelligence. Apart from the real-time operations, the proposed scheme also captures the operational planning, the verification of the energy and service provision, and the financial settlement. Although the case study is about a typical domestic appliance, the presented ideas support the large-scale implementation of demand response programs.

Simulation results show the potential of utilising demand response resources close to real-time for the provision of ancillary services to the system. The convergence of the aggregate demand response system under load frequency control is investigated, and the outcome is compared with actual market and performance data from conventional balance suppliers in The Netherlands. Simulation results show that the response of the aggregate demand response system outperforms that of conventional balance suppliers, both in terms of higher achieved correlation, but also in terms of faster time response.

Appendix

Real-Time Simulation Pseudo Code

1. **begin**;
2. # VTN is the aggregator, and VEN*j* the system users, with $j = 1, ..., N$.
3. # Current time instant is k, whereas $\tau = 4$ s, $n = 21\,600$, $i_{horizon} = 900$.
4. # The VTN obtains the power measurement $y_j(k)$ of the jth process, with $j = 1, ..., N$.
5. The VTN calculates the aggregate power output $y(k)$;
6. The VTN defines the processed set-point trajectory $s(k+i|k)$ for the considered control area by using (8)-(10);
7. # The VTN broadcasts the defined processed set-point trajectory $s(k+i|k)$ to all associated VEN*j* in the considered control area.
8. # Each associated VEN*j* obtains the broadcasted set-point trajectory.
9. **for** $j = 1$ to N **do**;
10. **for** $i = 1$ to $i_{horizon}$ **do**;
11. The VEN*j* creates the model-based prediction of the power output $p_{th,j}(k+i|k)$ under the standard thermostatic control;
12. **end for**;
13. Define the reference signal $r_j(k+i|k)$ of the jth process according to (4);
14. # Optimisation of the jth process: definition of the input trajectory $u_j(k+i|k)$ subject to the optimisation goal (5) and constraints (6) and (7).
15. **for** $i = 1$ to $i_{horizon}$ **do**;
16. **if** $s(k+i\,|\,k) > 0$ **then** $\min\limits_{u_j(k+i|k)} \left\{ r_j(k+i\,|\,k) \right\}$ **else**;
17. **if** $s(k+i\,|\,k) < 0$ **then** $\max\limits_{u_j(k+i|k)} \left\{ r_j(k+i\,|\,k) \right\}$ **else**;
18. **if** $s(k+i\,|\,k) = 0$ **then** $p_{MPC,j}(k+i\,|\,k) = p_{th,j}(k+i\,|\,k)$;
19. **end for**;
20. **for** $i = 1$ to $i_{horizon}$ **do**;
21. The VEN*j* creates the model-based prediction of the power output $p_{MPC,j}(k+i|k)$ under the MPC approach for the defined optimised input trajectory $u_j(k+i|k)$ in steps 15-19;
22. **end for**;
23. Calculate the reference trajectory $r_j(k+i|k)$, over the prediction horizon, i=1, ..., $i_{horizon}$, by using (4), and forward the result to the aggregator;
24. The VTN obtains the reference trajectory $r_j(k+i|k)$ from VEN*j*, performs consistency checks (e.g., overshooting avoidance) and sends back a binary signal notification signal $w_j(k) \in \{0,1\}$ to indicate rejection or acceptance with respect to $r_j(k+i|k)$;
25. In case of acceptance of the reference signal $r_j(k+i|k)$, the VEN*j* applies the first input to the jth process;
26. **end for**;
27. **for** $i = 1$ to $i_{horizon}$ **do**;
28. The VTN calculates the sum: $r(k+i\,|\,k) = \sum\limits_{j=1}^{N} r_j(k+i\,|\,k)$;
29. **end for**;
30. # The iteration continues with the next step and the process is repeated.
31. $k = k+1$;
32. **end**;

Acknowledgment

The authors acknowledge V. Ćuk for his contribution on this work through the provision of programming advices and assistance with the use of laboratory equipment.

References

[1] F. Rahimi and A. Ipakchi, "Demand response as a market resource under the smart grid paradigm," *IEEE Trans. Smart Grid*, vol. 1, no. 1, pp. 82–88, Jun. 2010.

[2] S. Stoft, *Power System Economics—Designing Markets for Electricity*. Hoboken, NJ, USA: IEEE Press & Wiley-Interscience, 2002.
[3] J. A. Short, D. G. Infield, and L. L. Freris, "Stabilization of grid frequency through dynamic demand control," *IEEE Trans. Power Syst.*, vol. 22, no. 3, pp. 1284–1293, Aug. 2007.
[4] S. A. Pourmousavi and M. H. Nehrir, "Real-time central demand response for primary frequency regulation in microgrids," *IEEE Trans. Smart Grid*, vol. 3, no. 4, pp. 1988–1996, Dec. 2012.
[5] D. Angeli and P.-A. Kountouriotis, "A stochastic approach to "dynamic-demand" refrigerator control," *IEEE Trans. Control Syst. Technol.*, vol. 20, no. 3, pp. 581–592, May 2012.
[6] I. Lampropoulos, J. Frunt, A. Virag, F. Nobel, P. P. J. van den Bosch, and W. L. Kling, "Analysis of the market-based service provision for operating reserves in The Netherlands," in *Proc. 9th Conf. Eur. Energy Market*, Florence, Italy, May 10–12, 2012, pp. 1–8.
[7] J. Kondoh, N. Lu, and D. J. Hammerstrom, "An evaluation of the water heater load potential for providing regulation service," *IEEE Trans. Power Syst.*, vol. 26, no. 3, pp. 1309–1316, Aug. 2011.
[8] N. Lu, "An evaluation of the HVAC load potential for providing load balancing service," *IEEE Trans. Smart Grid*, vol. 3, no. 3, pp. 1263–1270, Sep. 2012.
[9] A.-H. Mohsenian-Rad and A. Leon-Garcia, "Optimal residential load control with price prediction in real-time electricity pricing environments," *IEEE Trans. Smart Grid*, vol. 1, no. 2, pp. 120–133, Sep. 2010.
[10] A. J. Conejo, J. M. Morales, and L. Baringo, "Real-time demand response model," *IEEE Trans. Smart Grid*, vol. 1, no. 3, pp. 236–242, Dec. 2010.
[11] W. Hu, G.-P. Liu, and D. Rees, "Networked predictive control over the internet using round-trip delay measurement," *IEEE Trans. Instrum. Meas.*, vol. 57, no. 10, pp. 2231–2241, Oct. 2008.
[12] I. Lampropoulos, P. P. J. van den Bosch, and W. L. Kling, "A predictive control scheme for automated demand response mechanisms," in *Proc. IEEE PES Conf. Innovative Smart Grid Technologies (ISGT) Eur.*, Berlin, Germany, Oct. 14–17, 2012, pp. 1–8.
[13] N. Baghină, I. Lampropoulos, B. Asare-Bediako, W. L. Kling, and P. F. Ribeiro, "Predictive control of a domestic freezer for real-time demand response applications," in *Proc. IEEE PES Conf. Innovative Smart Grid Technologies (ISGT) Eur.*, Berlin, Germany, Oct. 14–17, 2012, pp. 1–8.
[14] ENTSO-E, "The Harmonised Electricity Market Role Model," Version: 2011-01, European Network of Transmission System Operators for Electricity [Online]. Available: http://www.ebix.org/Documents/role_model_v2011_01.pdf
[15] "Open Automated Demand Response (OpenADR) Communication Standards Development," Lawrence Berkeley National Laboratory, 2012 [Online]. Available: http://openadr.lbl.gov
[16] NXP Semiconductors, EM773 Energy Metering IC Product Data Sheet Rev. 2, Jan. 3, 2012 [Online]. Available: http://www.nxp.com/documents/data_sheet/EM773.pdf
[17] *IEEE Standard for Wireless Medium Access Control and Physical Layer Specifications for Low-Rate Wireless Personal Area Networks*, 802.15.4TM-2006, 2006, (Revision of IEEE Std 802.15.4-2003).
[18] MATLAB (Matrix Laboratory) Numerical Computing Environment and Programming Language, Mathworks, 2012 [Online]. Available: http:// www.mathworks.nl/products/matlab
[19] J. M. Maciejowski, *Predictive Control With Constraints*. Englewood Cliffs, NJ, USA: Prentice Hall, 2002.
[20] Y. Zong, D. Kullmann, A. Thavlov, O. Gehrke, and H. W. Bindner, "Application of model predictive control for active load management in a distributed power system with high wind penetration," *IEEE Trans. Smart Grid*, vol. 3, no. 2, pp. 1055–1062, Jun. 2012.
[21] P. Constantopoulos, F. C. Schweppe, and R. C. Larson, "ESTIA: A real-time consumer control scheme for space conditioning usage under spot electricity pricing," *Comput. Oper. Res.*, vol. 18, no. 8, pp. 751–765, Feb. 1991.
[22] APX Power NL, Day-Ahead Auction in The Netherlands [Online]. Available: http://www.apxendex.com/index.php?id=193
[23] A. Abdisalaam, I. Lampropoulos, J. Frunt, G. Verbong, and W. L. Kling, "Assessing the economic benefits of flexible residential load participation in the Dutch day-ahead spot and balancing markets," in *Proc 9th Conf. Eur. Energy Market*, Florence, Italy, May 10–12, 2012, pp. 1–8.
[24] R. Stamminger, Nov. 2008, Synergy Potential of Smart Appliances. University of Bonn. Bonn, Germany [Online]. Available: http://www.smart-a.org
[25] TenneT, Dutch Transmission System Operator, Data Export: Balance Delta With Prices Sep. 2012 [Online]. Available: http://www.tennet.org/english/operational_management/export_data.aspx
[26] K. M. Rogers, R. Klump, H. Khurana, and T. J. Overbye, "Smart-grid -enabled load and distributed generation as a reactive resource," in *Proc. 2010 IEEE PES Innovative Smart Grid Technologies (ISGT)*, Gaithersburg, MD, USA, Jan. 19–21, 2010, pp. 1–8.

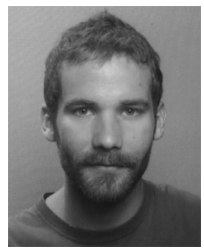

Ioannis Lampropoulos (S'10) received the Dipl. Ing. degree from the Department of Electrical and Computer Engineering, National Technical University of Athens, Greece, in 2006. In 2009, he received the M.Sc. degree in sustainable energy technology from Delft University of Technology, The Netherlands.

From February 2010 he is carrying out research at the group of Electrical Energy Systems, in Eindhoven University of Technology, The Netherlands. His research interests are in the areas of planning and operation of power systems, demand response, and renewable energy sources.

Mr. Lampropoulos has served as peer reviewer in international conference committees and IEEE Transactions. He is a registered engineer at the Technical Chamber of Greece since 2006, and he is a certified engineer in The Netherlands since 2009.

Nadina Baghină received the B.S. degree in electrical engineering and computer science from Jacobs University, Bremen, Germany, in 2010. In 2012, she received the M.Sc. degree in sustainable energy technology from Eindhoven University of Technology, The Netherlands, with a specialization in electrical energy systems.

Her research interests are in the areas of demand side management, demand response and management of distributed energy resources.

Wil L. Kling (M'95) received the M.Sc. degree in electrical engineering from the Technical University of Eindhoven, Eindhoven, The Netherlands, in 1978.

Since 1993, he has been a part-time professor in the Department of Electrical Engineering at Delft University of Technology, in the field of power systems engineering. Since 2008, he has been a full-time Professor at Eindhoven University of Technology, where he is leading research programs on distributed generation, integration of wind power, network concepts, and reliability.

Prof. Kling is involved in scientific organisations, such as CIGRE and the IEEE. As Netherlands' representative, he is a member of CIGRE Study Committee C6 Distribution Systems and Dispersed Generation and the Administrative Council of CIGRE.

Paulo F. Ribeiro (M'78–SM'88–F'03) received the B.S. degree in electrical engineering from the Universidade Federal de Pernambuco, Recife, Brazil, in 1975, completed the Electric Power Systems Engineering Course with Power Technologies, Inc. (PTI), in 1979, and received the Ph.D. degree from the University of Manchester, Manchester, U.K., in 1985.

Currently, he is with Eindhoven University of Technology, The Netherlands.

Dr. Ribeiro is active in the IEEE, CIGRE, and IEC technical working groups. He is a Registered Professional Engineer in the State of Iowa and an European Engineer (EurIng).